A promising plasma-catalytic approach towards single-step methane conversion to oxygenates at room temperature

Piu Chawdhury[1], Yaolin Wang[2], Debjyoti Ray[1], Stephanie Mathieu[2], Ni Wang[2], Jonathan Harding[2], Feng Bin[2,3], Xin Tu[2,*], Ch. Subrahmanyam[1,*]

[1] Department of Chemistry, Indian Institute of Technology Hyderabad, Telangana 502 285, India

[2] Department of Electrical Engineering and Electronics, University of Liverpool, Liverpool L69 3GJ, UK

[3] State Key Laboratory of High-Temperature Gas Dynamics, Institute of Mechanics, Chinese Academy of Sciences, Beijing 100190, China

Corresponding authors

Email: xin.tu@liverpool.ac.uk (X. Tu); csubbu@iith.ac.in (Ch. Subrahmanyam)

Abstract

Direct conversion of methane into chemicals and fuels under mild conditions has been considered as a 'holy grail' of chemistry and catalysis in the 21st century. Plasma-catalytic partial oxidation of methane (POM) to higher-value liquid fuels and chemicals over supported transition metal catalysts (Ni/γ-Al_2O_3, Cu/γ-Al_2O_3 and Fe/γ-Al_2O_3) has been investigated in a co-axial dielectric barrier discharge (DBD) reactor at room temperature and atmospheric pressure. The selectivity of oxygenates was ~58% in the plasma POM reaction without a catalyst, while the combination of DBD with the catalysts enhanced the selectivity of oxygenates to ~71%. Of the three catalysts, Fe/γ-Al_2O_3 showed the highest methanol selectivity of ~36% and a significant methanol yield of ~5%, while the use of Cu/γ-Al_2O_3 improved the selectivity of C_2 oxygenates to ~9%, which can be attributed to the presence of more acid sites on the surfaces of the Cu catalyst. The possible reaction pathways in the plasma-catalytic POM reaction have been explored by combined means of plasma electrical and optical diagnostics, analysis of gas and liquid products, as well as comprehensive catalyst characterization. The plausible reaction routes for the production of major oxygenate (methanol) on the Fe/γ-Al_2O_3 surfaces have been proposed. The surface CH_x species formed through the direct adsorption from CH_x radicals in the plasma gas-phase reactions via E-R mechanism or through the dissociation of adsorbed CH_4 on the surface are found to be crucial for methanol formation.

Keywords: Partial oxidation of methane; Non-thermal plasma; Plasma-catalysis; Methanol synthesis; Oxygenates

1. Introduction

Currently, the search for sustainable alternative resources is imperative as the world's energy consumption is still largely based on fossil fuels, leading to records in CO_2 emissions. In this context, the use of methanol as a substitute fuel has drawn much attention due to its renewable nature, high energy density and economic benefits [1]. The main feedstock for the synthesis of methanol is methane, the major component of natural gas with a high calorific value. A significant part of the world's primary energy consumption relies on its combustion for domestic heating and electrical power generation. However, direct conversion of methane to value-added chemicals and fuels under mild conditions is a 'holy grail' in chemistry and remains a challenge given that a large quantity of thermal energy is required to overcome the high stability of the C-H bonds [2]. Currently, the conversion of methane to liquid fuels and chemicals on a commercial scale is a two-step catalytic process. The first step is catalytic steam reforming of methane (SRM) to syngas (a mixture of CO and H_2) at high temperatures, while in the second step, syngas is catalytically converted to liquid fuels and chemicals (e.g. methanol) at relatively high temperatures and high pressures. High temperature and high-pressure two-step processes are energy-intensive and costly, limiting the sustainability of the process. Therefore, developing alternative and innovative energy-efficient technologies for direct transformation of methane to liquid chemicals such as partial oxidation of methane (POM) to oxygenates (e.g. methanol, R1) is highly desirable. Although considerable efforts have been made to investigating methane conversion to oxygenates using homogeneous or heterogeneous catalysis, the reported liquid yields (e.g. methanol) are still low and insufficient to compete with that from the conventional two-step process for methanol synthesis [3].

$CH_4 + ½\ O_2 \rightarrow CH_3OH \qquad \Delta H_{298K} = -126.4$ kJ/mol (R1)

Non-thermal plasma (NTP) has been regarded as a promising and emerging alternative to overcome these challenges, enabling methane activation at low temperatures and ambient pressure. Unlike thermal plasma, in an NTP, the electrical energy is exclusively used to generate highly energetic electrons and reactive species while keeping the gas kinetic temperature low [4]-[7]. A range of chemical reactions occur in NTPs as the molecules are activated by vibrational and electronic excitations which leads to their dissociation. In recent years, NTP has attracted increasing interest for the synthesis of fuels and chemicals via methane activation [8]-[12] and CO_2 conversion [13]-[19]. Dielectric barrier discharge (DBD) is one of the most commonly used NTP sources for chemical reactions especially plasma-catalytic process as DBD can be scaled up easily and is suitable for the combination with catalysts [19].

Most studies on plasma-assisted POM reaction focused on the production of syngas [20]-[21], while less attention has been placed on the direct and single-step synthesis of oxygenates (e.g. methanol) via POM. Zhou et al. investigated POM to methanol with oxygen or air using a DBD reactor and found that the formation of H_2O and CO showed a strong negative influence on methanol formation [22]. The optimum methanol selectivity of ~30% was achieved at an oxygen concentration of ~15% in both CH_4/O_2 and CH_4/air mixtures [22]. Nozaki and co-workers developed an NTP microreactor for a single step and room temperature synthesis of oxygenates (methanol, formaldehyde and formic acid) via POM with a one-pass liquid yield of 5-20% and a selectivity of 70-30% [23]. Other oxidants such as CO_2 and N_2O have also been reported for plasma-assisted POM to oxygenates. Zou et al. used CO_2 as a soft oxidant for the plasma oxidation of methane to oxygenates (formaldehyde, methanol, ethanol, formic acid and acetic acid) with a total oxygenate selectivity of up to 41% [24]. Indarto et al. reported a methanol selectivity of 32%

in the plasma POM with NO_2 using a DBD reactor [25]. Subrahmanyam and co-workers also investigated plasma-assisted POM with N_2O for the synthesis of methanol [9][26].

The combination of NTP with a catalyst has great potential to effectively enhance the reaction performance through the plasma-catalyst synergy. Compared to extensive research on plasma-catalytic conversion of methane to gas products (e.g. syngas), very limited attention has been placed on the direct conversion of methane to liquid oxygenates using plasma-catalysis. Chen et al. investigated plasma-catalytic POM over a Cu-promoted iron oxide catalyst using both in-plasma catalysis (IPC) and post-plasma catalysis (PPC). A synergistic effect of plasma catalysis was found with a maximum CH_3OH yield of 1.6% when using the IPC configuration [27]. Indarto et al. showed that the presence of a copper-zinc-alumina (CZA) catalyst doubled the methanol selectivity compared to the plasma POM reaction without a catalyst [28]. The same group found using yttria-stabilized zirconia (YSZ) as a catalyst support led to higher methanol selectivity in the plasma-catalytic POM compared to other supports including Al_2O_3, TiO_2, SiO_2, Carbon and ZSM-13. The highest methanol selectivity (~23%) was achieved when using a Ni/YSZ catalyst, which can be attributed to the change of the reaction mechanism due to the presence of more surface oxygen vacancies on the YSZ surface [29]. Recently, Wang et al. developed a single-step plasma-catalytic process for the direct conversion of CH_4 with CO_2 to a range of liquid fuels and chemicals (e.g. acetic acid, methanol, ethanol, acetone and formaldehyde) at room temperature and atmospheric pressure. The synergistic effect of plasma and Cu/γ-Al_2O_3 significantly increased the total selectivity of oxygenates to 50-60%, with acetic acid being the major liquid product with a selectivity of 40.2% [30]. Li et al. also investigated the direct conversion of CH_4 and CO_2 into liquid chemicals (mainly methanol and acetic acid) using SiO_2 aerogel supported Co and Fe catalysts in a DBD reactor and reported a total oxygenate selectivity of 40% [31]. Up until now,

the reported selectivities and yields of liquid chemicals in the plasma-catalytic POM process remain low due to the limited knowledge of selecting and designing cost-effective, highly active and stable catalysts that are effective in plasma-catalytic oxidation of methane to oxygenates. A better fundamental understanding of the plasma-catalysts interactions is essential for the development of optimized catalysts in the selective synthesis of oxygenates.

Catalysts effective in similar thermal reactions are often used as a starting point of plasma-catalytic reactions. Cu-based catalysts have been extensively investigated in catalytic methane oxidation due to high activity of Cu towards methanol synthesis [32]. Fe-based catalysts have also received considerable attention for the catalytic oxidation of methane to oxygenates [33]. Ni is the most widely used metal catalyst due to its availability and low cost. Supported Ni catalysts have been extensively evaluated for catalytic methane activation to value-added fuels and chemicals. Compared to thermal catalytic POM to oxygenates, only a few catalysts have been evaluated in the direct POM to oxygenates using plasma catalysis. To the best of our knowledge, the effect of different cost-effective supported transition metal catalysts on the plasma-catalytic oxidation of methane to oxygenates has not been explored yet. A fundamental understanding of the catalyst properties in the low-temperature plasma-catalytic oxidation of methane to oxygenates is still very limited. Therefore, it is important to get new insights into the plasma-catalyst interactions in the direct oxidation of methane to liquid fuels and chemicals under mild conditions.

In this study, plasma-catalytic partial oxidation of methane to liquid oxygenates has been carried out at ambient temperature and atmospheric pressure using a co-axial DBD plasma reactor. The effect of γ-Al_2O_3 supported metal oxide catalysts (Ni, Cu and Fe) on the plasma-catalytic POM has been investigated in terms of the conversion of methane, the selectivity of gas products and oxygenates and the energy efficiency of the process. A comprehensive catalyst characterization

has been performed to establish the links between the catalyst properties and the reaction performance. Optical emission spectroscopic (OES) diagnostics has been employed to understand the formation of reactive species in the plasma-catalytic POM reaction. The plausible reaction pathways in the plasma-catalytic POM reaction have been proposed and discussed.

2. Experimental Section

2.1. Experimental setup

Fig. 1 shows the schematic diagram of the experimental setup. A quartz tube with an inner diameter of 20 mm and an outer diameter of 23 mm was used as a dielectric for the DBD reactor. A stainless steel (SS) rod with an outer diameter of 9 mm was placed along the axis of the quartz tube as a high voltage electrode, while a 9-cm long SS mesh was wrapped around the quartz tube and served as a ground electrode. The discharge gap was kept at 5.5 mm with a discharge length of 7 cm in the experiments. The DBD reactor was connected to an alternating current (AC) high voltage power generator with a variable peak voltage of 14-22 kV at a fixed frequency of 50 Hz. A mixture of CH_4 and O_2 was supplied to the reactor at a constant flow rate of 30 ml min^{-1} with a CH_4/O_2 molar ratio of 5:1. In the plasma-catalytic reaction, 1.5 g catalyst was fully packed inside the discharge gap, and the volume of the catalyst bed was around 15 ml. An Agilent 34136A high voltage probe was connected to the inner electrode to measure the applied voltage, while a four-channel digital oscilloscope (Tektronix TDS2014B) was used to record the electrical signals. The discharge power was determined using the typical Q-U Lissajous figure method. As the discharge power was quite low (1.8 W) and constant throughout the experiment, the reaction temperature of the plasma process can be maintained at room temperature and was almost the same when using different catalysts. The gaseous products were analyzed using a gas chromatograph (Shimadzu GC-2014) equipped with a packed column (HayeSep A, 80/100 mesh, 3 m) and a thermal

conductivity detector (TCD). The liquid products were condensed and collected in an ice-cold trap placed at the exit of the DBD reactor. The liquid oxygenates were qualitatively analyzed using gas chromatography-mass spectrometry (GC-MS) (Thermo Scientific Trace GC Ultra) and quantitatively analyzed using a gas chromatograph (Thermo Scientific Trace GC Ultra) equipped with a flame ionization detector (FID) with a DB-WAX column. An infrared CO_x analyzer (Fuji Electric, Japan) was used to monitor the formation of CO and CO_2 in the reaction. The measurements started after running the reaction for 1.5 h. To evaluate the reaction performance, the concentration of the liquid products in the condensate was calculated using the corresponding formula of the standard calibrated concentration curve (see Table S1 in Supplementary Materials). The emission spectra of the discharge were recorded by an emission spectrometer (Princeton Instruments, Acton SpectraPro SP-2300) in the range of 200 - 800 nm, using an optical fiber placed close to the SS mesh (ground electrode) of the DBD reactor.

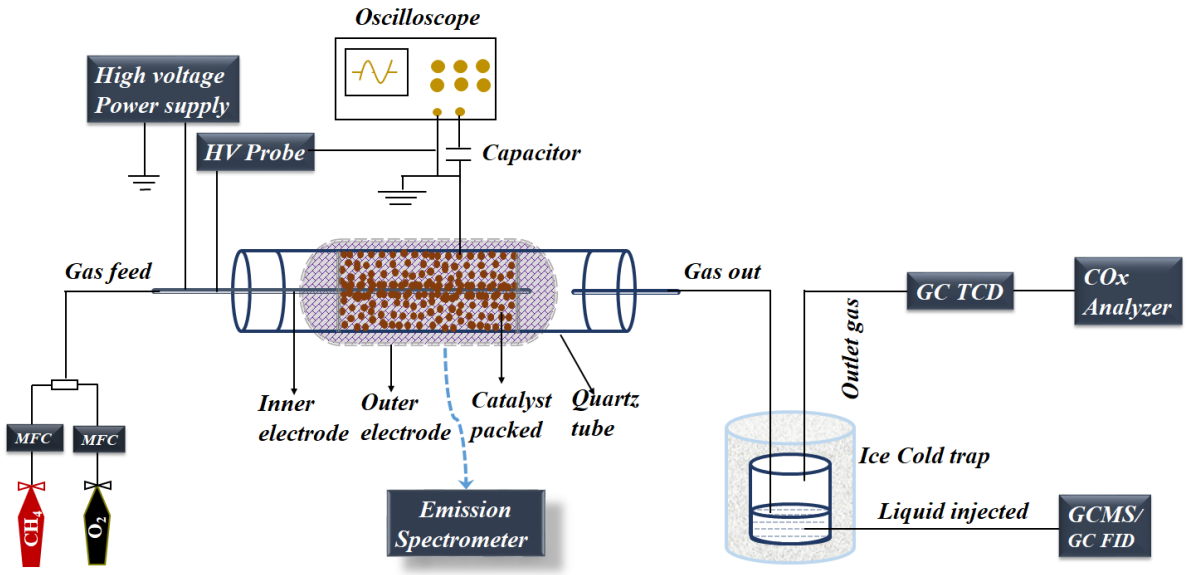

Fig.1. Schematic diagram of the experimental setup.

In this work, the conversion of CH_4 and the selectivity of the gaseous products (CO_x, C_2H_6 and H_2) are calculated as follows:

$$CH_4\ conversion\ (\%) = \frac{Number\ of\ moles\ of\ CH_4\ converted}{Number\ of\ moles\ of CH_4\ input} \times 100 \quad (1)$$

$$Selectivity\ of\ CO_x(\%) = \frac{Number\ of\ moles\ of\ CO_x\ produced}{Number\ of\ moles\ of\ CH_4\ converted} \times 100 \quad (2)$$

$$Selectivity\ of\ C_2H_6\ (\%) = \frac{2 \times Number\ of\ moles\ of\ C_2H_6\ produced}{Number\ of\ moles\ of\ CH_4\ converted} \times 100 \quad (3)$$

$$Selectivity\ of\ H_2\ (\%) = \frac{Number\ of\ moles\ of H_2\ produced}{2 \times Number\ of\ moles\ of\ CH_4\ converted} \times 100 \quad (4)$$

The total selectivity of oxygenates is defined as:

$$Total\ selectivity\ of\ oxygenates\ (\%) = 100 - (S_{CO} + S_{CO_2} + S_{C_2H_6}) \quad (5)$$

Where S_{CO}, S_{CO_2} and $S_{C_2H_6}$ are the selectivity of CO, CO_2 and C_2H_6, respectively.

The selectivity of oxygenate i can be determined as

$$S_i(\%) = \frac{n_i C_i}{\sum n_i C_i} \times Eq\ (5) \quad (6)$$

Where n_i is the number of carbon moles of the oxygenate i, C_i is the concentration of the oxygenate i.

The yield of the products is given by:

$$Yield\ (\%) = Selectivity \times CH_4\ conversion\ (\%) \quad (7)$$

The energy efficiency for the conversion of methane is determined by:

$$Energy\ efficiency\ for\ CH_4 conversion\ (mmol/kJ)$$

$$= \frac{CH_4\ converted\ \ (mmol/\min)}{Discharge\ power\ (W)} \times \frac{1000}{60} \quad (8)$$

2.2. Catalyst preparation

All the catalysts were synthesized by the incipient wetness impregnation method. The metal precursor solutions were prepared by dissolving each metal salt ($Cu(NO_3)_2 \cdot xH_2O$; $Fe(NO_3)_3 \cdot 9H_2O$ or $Ni(NO_3)_2 \cdot 6H_2O$) in an amount of water just sufficient to fill the pores of the γ-Al_2O_3 support. The γ-Al_2O_3 was first calcined at 400 °C for 5 h to remove all the impurities (e.g., adsorbed H_2O), then it was added to the precursor solution and stirred until thoroughly mixed. The resulting mixture was kept at room temperature for 3 h and then dried overnight at 80 °C. Finally, the dried sample was calcined at 500 °C for 4 h and then sieved to a particle diameter of 40 - 60 mesh. The metal (Cu, Fe or Ni) loading of the prepared catalysts was ~ 9 wt.%.

2.3. Catalyst characterization

The composition of the prepared catalysts was confirmed through powder X-ray diff raction (XRD) by using an X-ray diff ractometer (Panalytical X'PERT PRO) with a Cu Kα radiation source (λ = 1.541 Å) at a scan rate of 0.01670° s^{-1}. The physisorption properties of the catalysts were determined using N_2 adsorption/desorption measurements on an automated gas sorption analyzer (NOVA2200e, Quantachrome, USA) at a constant liquid nitrogen temperature of 77 K. Prior to the analysis, all the samples were pre-treated by degassing at 300 ^oC for 3 h under vacuum. Temperature programmed reduction of hydrogen (H_2-TPR) and temperature-programmed desorption of NH_3 (NH_3-TPD) and CO_2 (CO_2-TPD) experiments were carried out using a chemisorption apparatus (MicrotracBEL Corp.) equipped with a TCD detector. For the H_2-TPR analysis, the sample (~80 mg) was pre-treated in a He flow at 300 ^oC for 50 min and then cooled

to room temperature under flowing Ar. The TPR profile was recorded when heating the sample to the target temperature of 900 ^{o}C at a constant ramping rate of 10 ^{o}C min^{-1} in a 5 vol.% H_2/Ar gas flow. The reduction signal obtained was compared to the pre-calibrated signal for quantitative analysis. To investigate the acidic properties of the catalysts, NH_3-TPD experiments were carried out. After the pre-treatment of the samples at 500 ^{o}C for 1 h under flowing He, the sample (~80 mg) was cooled to 100 ^{o}C followed by adsorption of NH_3 in a flow of 5 vol.% NH_3/He at 100 ^{o}C. The desorption process was performed upon the heating of the sample to the target temperature of 500 ^{o}C at a constant heating rate of 10 ^{o}C min^{-1} under a He flow of 30 ml min^{-1}. The basic properties of the catalysts were examined using CO_2-TPD analysis. Prior to the measurement, the sample (~80 mg) was pre-treated under a He flow for 1 h at 300 ^{o}C followed by a cooling process to 100 ^{o}C and the simultaneous adsorption of CO_2 in a 10 vol.% CO_2/He mixture gas at the same temperature. Then, the sample temperature was raised to 800 ^{o}C at a heating rate of 10 ^{o}C min^{-1} under a He flow of 30 ml min^{-1} to allow the desorption to proceed. The CH_4-TPD experiment was performed in the same way with He pre-treatment followed by the adsorption of 10 vol.% CH_4/He mixture gas. The desorption process occurred after the sample temperature reached 800 ^{o}C at a constant He flow of 50 ml min^{-1}. The morphologies of the catalysts were characterized by high-resolution transmission electron microscopy (HRTEM) measurements using a JEOL-2100 TEM model operated at 200 kV. The thermal gravimetric analysis (TGA) of the fresh and spent catalysts was performed using an SDT Q600 instrument (TA Instruments, USA). The TGA analysis was recorded in an O_2 atmosphere heated to 900 ^{o}C at a heating rate of 10 ^{o}C min^{-1}. The metal loading of the prepared catalysts was determined by using inductively coupled plasma optical emission spectroscopy (ICP-OES) analysis with a Prodigy high dispersion ICP (Teledyne Instruments, USA).

3. Results and discussion

3.1. Catalyst characterization

3.1.1. XRD analysis

Fig. 2 shows the XRD patterns of the fresh catalysts. All the catalysts show three major diffraction peaks at 2θ = 37.7º, 45.9º and 67.0º corresponding to the (311), (400) and (440) planes of the cubic structure of crystalline γ-Al_2O_3 (JCPDS reference No. 00-010-0425). The XRD pattern of the Cu/γ-Al_2O_3 catalyst exhibits some distinctive characteristic peaks at 2θ = 32.5º, 35.5º, 38.6º, 48.7º, 58.3º, 61.6º and 75.2º with corresponding d-spacing values of 0.274 nm, 0.252 nm, 0.232 nm, 0.186 nm, 0.158 nm, 0.150 nm and 0.126 nm, which can be indexed to the (110), (-111), (111), (-202), (202), (-113) and (-222) planes of the monoclinic CuO crystalline phase, respectively, according to the standard JCPDS file No. 89-5898. In addition to the formation of the CuO crystallite, some characteristic peaks at 2θ = 19.3º and 27.7º corresponding to the (200) and (220) planes of Cu_2O evidence the presence of two oxidation states of copper, as confirmed by the JCPDS No. 34-1354. The average crystallite size of CuO is 9.6 nm, calculated using the Scherrer's equation to the (111) plane. The XRD pattern of Fe/γ-Al_2O_3 shows multiple peaks at 2θ = 24.1º, 33.1º, 35.6º, 40.8º, 49.4º, 54º, 57.6º, 62.4º, 63.9º,72.3º, 75.4º, 84.9º and 88.7º corresponding to the respective planes of (012), (104), (110), (113), (024), (116), (018), (214), (300), (119), (220), (134) and (226), confirming the formation of a rhombohedral Fe_2O_3 phase on the γ-Al_2O_3 support, as described in the JCPDS file No. 89-2810. Using the same method, the average crystallite size of Fe_2O_3 is 15.4 nm, determined from the high-intensity peak of the (104) plane. The diffraction peaks for the Ni/γ-Al_2O_3 catalyst at 2θ = 43.3º and 62.9º, corresponding to an interplanar distance of 0.208 nm and 0.147 nm, can be attributed to the (200) and (220) planes of the cubic crystal structure of NiO (JCPDS No. 04-0835). Therefore, the XRD patterns of the catalysts confirm the

formation of metal oxide crystallites on the γ-Al_2O_3 supports, as expected after the catalyst calcination.

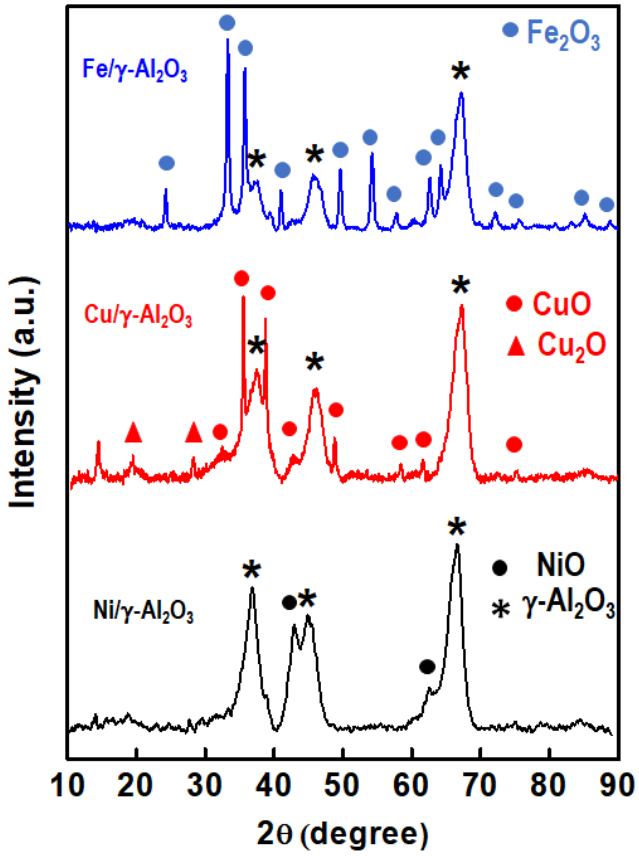

Fig.2. XRD patterns of the fresh catalysts.

3.1.2. Physisorption properties of the catalysts

The results of the N_2 adsorption-desorption analysis on the synthesized catalysts are summarized in Table 1. It can be seen that the Cu/γ-Al_2O_3 catalyst shows a higher specific surface area in comparison to the other two catalysts, while they do not differ much in average pore diameters and average pore volumes. These results are in accordance with the observation of the adsorption-desorption isotherms plotted in Fig. 3. All the catalysts exhibit a typical Type-V isotherm with an H3-type hysteresis loop at a relative pressure P/P_0 of 0.4 to 0.9, which indicates the presence of

mesopores in the catalysts. The lower specific surface area of the Fe/γ-Al_2O_3 catalyst can be ascribed to the larger size of the Fe_2O_3 particles formed on the γ-Al_2O_3 surface (Fig. S1).

Table 1. Physio-chemical properties of the fresh catalysts.

Catalyst	S_{BET} (m^2 g^{-1})[a]	V_{BJH} (cc g^{-1})[b]	D_{BJH} (nm)[b]	Metal content (%)[c]
γ -Al_2O_3	295	0.62	3.7	-
Ni/γ-Al_2O_3	248	0.51	3.6	9
Cu/γ-Al_2O_3	274	0.54	3.6	9.2
Fe/γ-Al_2O_3	235	0.44	3.5	9.2

[a] The specific surface area of the catalysts was calculated from the Brunauer–Emmett–Teller (BET) method.

[b] The average pore volumes and pore diameters of the catalysts were measured from the Barrett-Joyner-Halenda (BJH) method.

[c] The metal loading on γ-Al_2O_3 support was determined using ICP-OES.

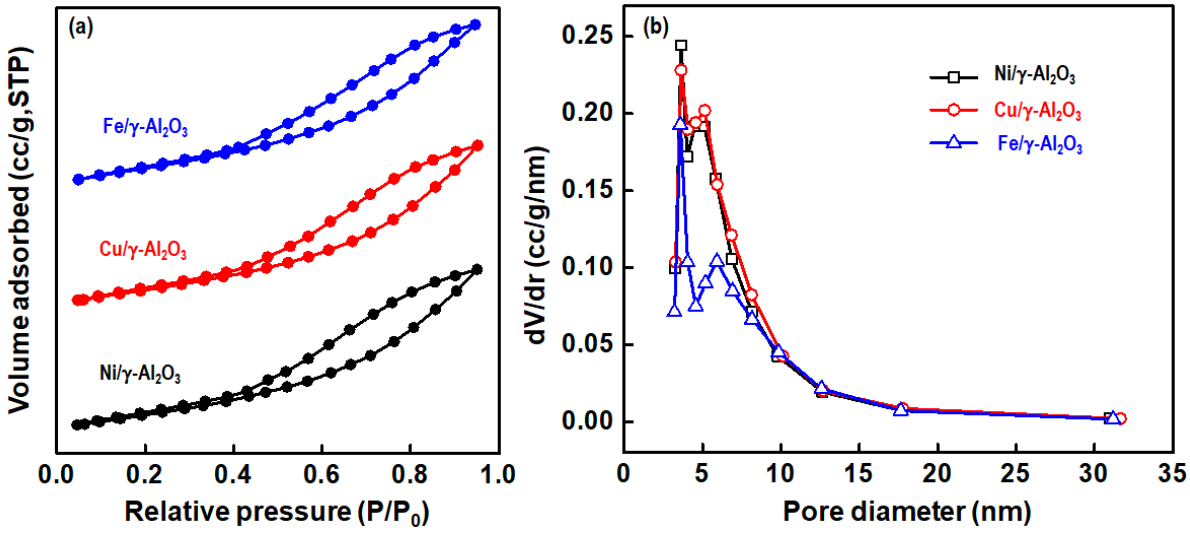

Fig. 3. (a) N_2 adsorption-desorption isotherms of the fresh catalysts. (b) Pore size distribution of the fresh catalysts.

3.1.3. H_2-TPR analysis

H_2-TPR analysis of the catalysts was carried out to investigate the metal-support interactions and the redox properties of the catalysts. As seen in Fig. 4, several peaks of H_2 consumption arise at different temperatures for each catalyst. These peaks are linked to the different oxidation states of the metals and thus demonstrate the strong interaction that exists between the metals and the supports. The first reduction peak of the Cu/γ-Al_2O_3 catalyst at 225 ^oC with an H_2-consumption of 0.578 mmol g^{-1} can be attributed to the stepwise reduction of surface dispersed CuO nanoparticles (to Cu^0 state) and the partial reduction of surface interacted Cu^{+2} (to Cu^+); while the 2nd peak is associated with the reduction of part of the supported Cu^+ and the bulk crystalline CuO with a total H_2-consumption of 0.321 mmol g^{-1} [34][35]. The total H_2-consumption for the Ni-based catalyst was 1.388 mmol g^{-1}. The reducible NiO species of the Ni/γ-Al_2O_3 catalyst can be classified into four types, including low temperature (up to 400 ^oC) peaks α, medium temperature peaks β (400 - 500 ^oC), high temperature peaks γ_1 (540 - 700 ^oC) and very high temperature peaks γ_2 (>750 ^oC)

[36]. Each set of peaks corresponds to different states of NiO species. The peaks in the low temperature range (up to 400 ^{o}C) can be assigned to α-type NiO species, which are attributed to the reduction of free NiO dispersed on the surface of the γ-Al_2O_3 support and having no or very limited interaction with the support. The medium temperature peak (400 -500 ^{o}C) represents β-type NiO species, which have a stronger interaction with the γ-Al_2O_3 support than the α-type NiO [36]. The high temperature peaks (540 - 700 ^{o}C) were assigned to γ_1-type NiO species, which are a stable nickel aluminum phase. The very high temperature peak γ_2-type at >750 ^{o}C is assigned to the reduction of a diluted $NiAl_2O_4$-like phase, formed through the diffusion of nickel ions into the γ-Al_2O_3 support [36]. There are two distinct reduction temperature zones appearing in the TPR profile of the Fe/γ-Al_2O_3 catalyst which occurred through the stepwise reduction of Fe_2O_3 → Fe via Fe_3O_4 with a total H_2-uptake of 0.879 mmol g^{-1}. The first broad peak located in the temperature range from 250 to 500 ^{o}C is ascribed to the stepwise reduction of the iron species Fe_2O_3 → Fe_3O_4 → FeO. The peak at 440 ^{o}C typically represents the Fe_3O_4 → FeO transformation [37][38]. The latter peaks in the temperature region from 580 to 800 ^{o}C can be ascribed to the reduction of Fe_3O_4 → metallic Fe via the formation of FeO [39]. Generally, a lower onset reduction temperature of the catalyst results from the formation of larger metal oxide crystallites on the catalyst surface [40]. The strong metal-support interaction promotes the distribution of the metal oxide species on the catalyst, which affects the catalyst characteristics [41].

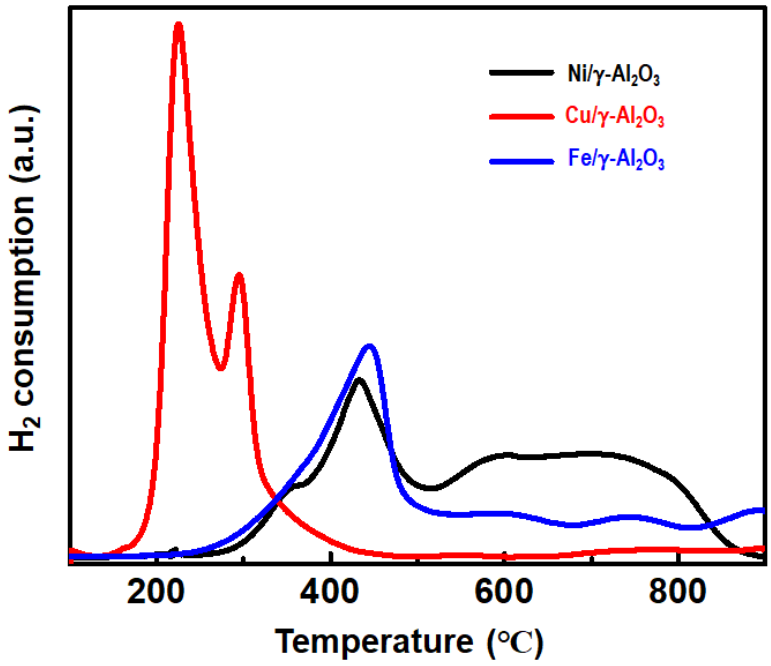

Fig. 4. H_2-TPR profiles of the fresh catalysts.

3.1.4. NH_3-TPD analysis

The acidic nature of the catalysts was evaluated by the NH_3-TPD experiment in which NH_3 was adsorbed on the catalyst surface at low temperature owing to the acidic character of the catalyst, and then desorbed at higher temperatures. The TPD profiles of the prepared catalysts slightly differ from each other in the temperature zone (110 - 440 °C) of the NH_3 desorption, as suggested by Fig. 5. It can be seen that both the Ni/γ-Al_2O_3 and Fe/γ-Al_2O_3 catalysts show a strong, wide peak of NH_3 desorption in the region of 110 to 440 °C, while two consecutive peaks of desorption centered at 197 °C and 282 °C are exhibited by the Cu/γ-Al_2O_3 catalyst in the same temperature range. Hence, the catalysts can be ordered according to their acidity in the sequence: Cu/γ-Al_2O_3 > Ni/γ-Al_2O_3 > Fe/γ-Al_2O_3, in agreement with the results shown in Table S2.

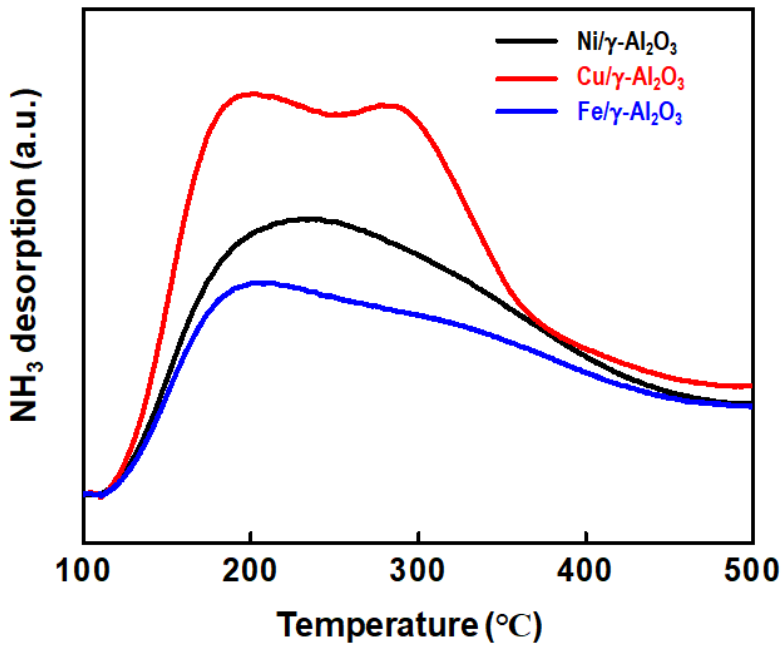

Fig. 5. NH_3-TPD profiles of the fresh catalysts.

3.1.5. CO_2 -TPD analysis

Fig. 6 presents the CO_2-TPD profiles of the synthesized catalysts when CO_2 was adsorbed at 100 ^oC and underwent the desorption process at high temperature, up to 800 ^oC. The desorption profiles reveal three types of CO_2 desorption peaks in the temperature ranges of 110- 317 ^oC, 320 - 440 ^oC and 450- 770 ^oC corresponding to weak, moderate and strong basic sites of the catalysts, respectively. From the amounts of CO_2 desorbed listed in Table S3, it can be deduced that the sequence in terms of their basicity is as follows: Fe/γ-Al_2O_3 > Ni/γ-Al_2O_3 > Cu/γ-Al_2O_3, which corroborates the above acidity order. All the catalysts possess basic sites which are dense and weak in the lower temperature range, strong and broad in the higher temperature region and moderate in the mid-temperature range. The lower temperature peak results from the formation of bicarbonate species through the reaction of CO_2 with surface -OH groups, while the formation of bidentate and monodentate carbonate species generated through metal-oxygen pairings are responsible for the

higher temperature peaks [42]. Among the weak and moderate basic sites of the catalysts, those of Fe/γ-Al_2O_3 shows the highest amount of CO_2 adsorbed (through the reaction with surface –OH groups), while Ni/γ-Al_2O_3 holds the strongest basic site at high temperature (Table S3).

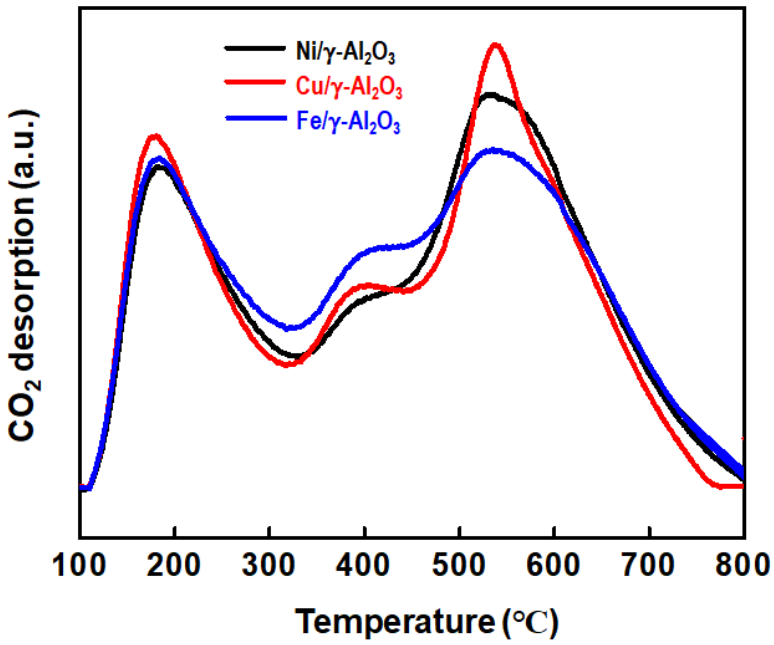

Fig. 6. CO_2 -TPD profiles of the fresh catalysts.

3.1.6. Morphology analysis of the catalysts

Fig. 7 shows the HRTEM images of the prepared catalysts. The γ-Al_2O_3 support has a fibrous structure, which is supposed to allow a homogenous distribution of the metal oxide particles. Though the changes in the shape of the metal oxide particles are not visible, it is possible to distinguish dark spots over the γ-Al_2O_3 support, which are irregular in size and shape and differ for the three catalysts (Fig. 7a, d and g). From the particle distribution curves shown in Fig. S1, the average size of metal oxide in the Ni, Cu and Fe catalysts is 10.3, 9.9 and 13.0 nm, respectively, which is consistent with the XRD results. The HRTEM image of Ni/γ-Al_2O_3 shows perfect lattice

fringes of 0.208 nm (Fig. 7b) corresponding to the (202) plane of the NiO crystallite, while the selected area electron diffraction (SAED) pattern analysis confirms the high crystallinity of the NiO catalyst (Fig. 7c). Moreover, the lattice planes obtained from the SAED pattern (Fig. 7c) correspond well with the XRD results. The interplanar distance between the CuO lattice fringes was calculated to be 0.232 nm (Fig. 7e), corresponding to the (111) plane of the monoclinic CuO phase. This result is supported by the SAED pattern analysis (Fig. 7f). The fuzzy fringes formed by the Fe_2O_3 particles, obtained from the lattice-scale image of the Fe/γ-Al_2O_3 catalyst, present an interfringe distance of 0.252 nm which originates from the crystalline (110) plane (Fig. 7h). The SAED pattern confirms the formation of the rhombohedral phase of Fe_2O_3 with the presence of reflection planes in the SAED pattern (Fig. 7i).

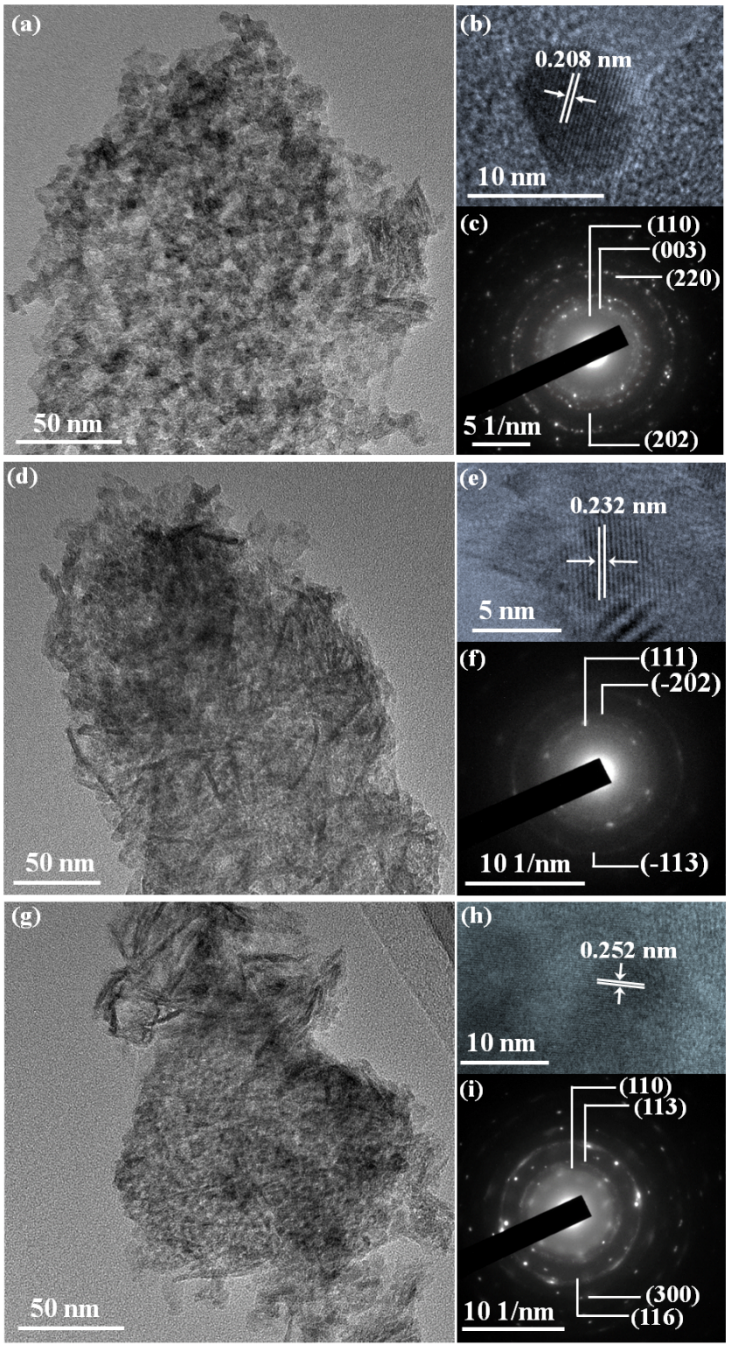

Fig. 7. HRTEM images of the fresh catalysts, (a) Ni/γ-Al_2O_3; (d) Cu/γ-Al_2O_3; (g) Fe/γ-Al_2O_3; Lattice-scale images of the catalysts (b) Ni/γ-Al_2O_3; (e) Cu/γ-Al_2O_3; (h) Fe/γ-Al_2O_3; SAED patterns of (c) NiO; (e) CuO; (i) Fe_2O_3.

3.2. Effect of catalysts on the discharge characteristics

The plasma discharge properties are determined from the Lissajous figure (Fig. 8a) and listed in Table 2. There is a notable difference in the discharge parameters when the plasma operates with or without a catalyst. Although the parameters do not vary much when they are compared among the catalysts themselves, introducing metal loading on γ-Al_2O_3 enhanced the average electric field compared to the DBD packed with γ-Al_2O_3. As a consequence, the reaction performance is also influenced. At a constant discharge power of 1.8 W, the combination of plasma with the Fe/γ-Al_2O_3 catalyst reduced the breakdown voltage and hence allowed the reaction to effectively initiate with the observation of the reactant decay. As dielectric materials effectively accumulate charges on their surface, the metal oxide loaded γ-Al_2O_3 catalysts act in the same way, therefore improving the charge transfer between the electrodes. The methods to calculate the discharge parameters are given in the Supplementary Material (Section S5 & Fig. S2). Compared to the plasma reaction without packing, the presence of γ-Al_2O_3 in the DBD slightly increased the average electric field from 7.8 kV cm^{-1} (plasma only) to 8.2 kV cm^{-1}, while the coupling of DBD with Fe/γ-Al_2O_3 further increased the average electric field to 8.7 kV cm^{-1}. An improvement in the reduced electric field was also observed when placing support or Fe/ γ-Al_2O_3 in the DBD, which follows the order: plasma + Fe/γ-Al_2O_3 > plasma + γ-Al_2O_3 > plasma only. This finding can be attributed to the increase of charge deposition allowed by the dielectric catalyst materials. Indeed, the enhancement of the charge transfer is due to the increased strength of the local electrical field at the contact points between the packed catalysts and the catalyst-dielectric wall. The mean electron energy and the electron energy distribution function (EEDF) were calculated using the Boltzmann equation solver software BOLSIG+ [43]. The mean electron energy of the discharge followed the order: plasma only < plasma + γ-Al_2O_3 < plasma + Fe/γ-Al_2O_3, which correlates well with the order of

the reduced electric field. Fig. 8b shows the variation of the mean electron energy as a function of the reduced electric field (E/N) for both the plasma-only and the plasma-catalytic processes, as plotted in Fig. 8c. We can observe that the catalyst addition in the discharge zone results in the generation of more energetic electrons with higher energy (Fig. 8c).

The rate coefficients for the most common gas-phase electron-impact reactions in the CH_4 - O_2 plasma system were also studied using BOLSIG+. As shown in Fig. S3, the rate coefficients of the reactions increase with increasing E/N values. A series of gas-phase vibrational excitation and dissociation reactions are considered and listed in Table S4. As expected, in the DBD packed with Fe/γ-Al_2O_3, the increase of the reactions rates with the reduced electric field is even more pronounced in comparison to the plasma reaction with no packing. This finding suggests that the increase of E/N and mean electron energy positively affects the generation of highly reactive species (e.g., radicals) through a series of electron-impact reactions which can effectively speed up the reactions to the desired products.

Table 2. Effect of γ-Al_2O_3 and Fe/γ-Al_2O_3 on the characteristics of the discharge.

Plasma mode	U_b (kV)	Q_{pk-pk} (μC)	dQ (μC)	C_{cell} (μF)	C_d (μF)	E (kV/cm)	E/N (Td)
Plasma only	4.3	6.5	5.2	0.09	0.64	7.8	29
Plasma + γ-Al_2O_3	3.8	9.0	7.1	0.11	0.72	8.2	30.5

Plasma + $Ni/\gamma\text{-}Al_2O_3$	4.1	9.5	7.4	0.11	0.74	8.5	32
Plasma + $Cu/\gamma\text{-}Al_2O_3$	4.2	9.2	7.0	0.11	0.75	8.9	33.2
Plasma + $Fe/\gamma\text{-}Al_2O_3$	4.1	9.2	7.2	0.12	0.71	8.8	33

U_b = Breakdown voltage

$Q_{pk\text{-}pk}$ = Peak to peak charge

dQ = Charge transfer per half cycle

C_{cell} = Cell capacitance

C_d = Dielectric capacitance

E = Average electric field

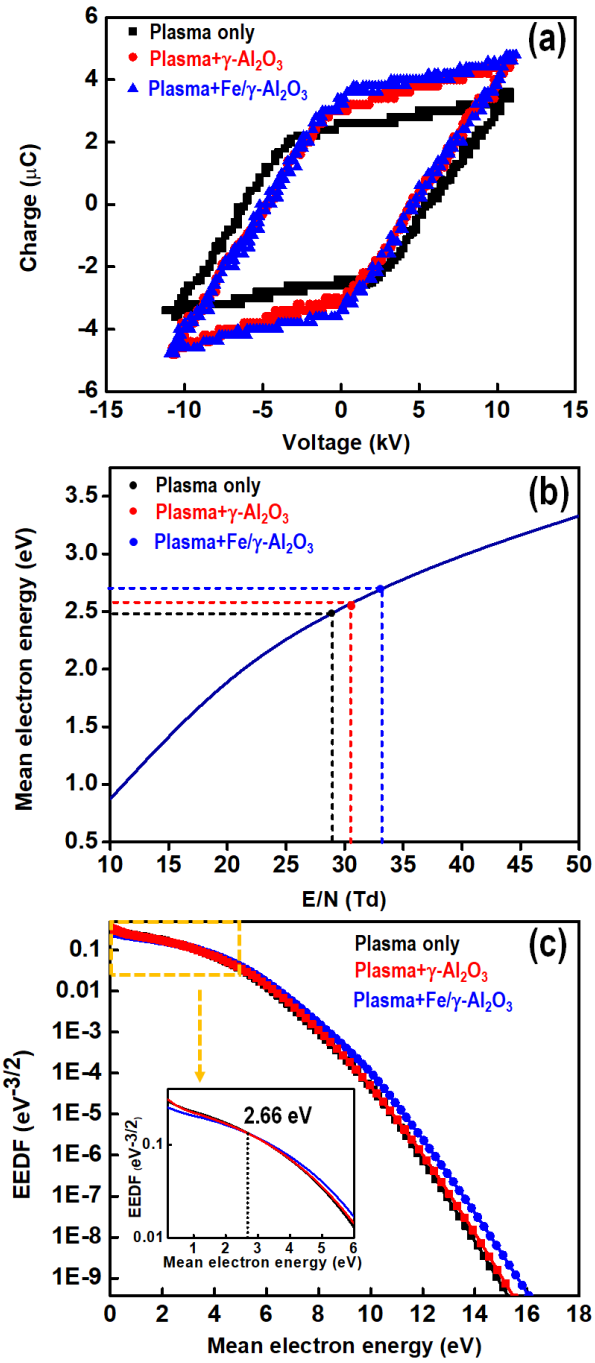

Fig. 8. (a) Lissajous figures of the discharge; (b) Calculated mean electron energy versus E/N; (c) Variation of EEDF as a function of the mean electron energy.

3.3. Plasma-catalytic partial oxidation of methane

Fig. 9 shows the effect of the catalysts and support on the selectivity of gaseous and liquid products in the plasma-catalytic POM reaction. In the plasma reaction without a catalyst (Plasma only), H_2 was the major gaseous product with a selectivity of 33%, followed by C_2 hydrocarbons with a selectivity of 17%. A very low amount of CO_2 was detected, as expected in the partial oxidation of methane. In the absence of a catalyst, HCHO, CH_3OH and HCOOH were found to be the dominant oxygenates in the liquid products with a selectivity of 10%, 20% and 25%, respectively. Clearly, the combination of DBD with the catalysts affects both the conversion of CH_4 and the selectivity of the products. Compared to the reaction using plasma only (Fig. 9), adding γ-Al_2O_3 to the DBD slightly increased the conversion of methane and energy efficiency, but did not substantially enhance the selectivity of oxygenates (especially for methanol, formaldehyde and formic acid). This result can be explained by the limited catalytic selectivity of γ-Al_2O_3. Interestingly, the coupling of DBD with metal oxide catalysts decreased the total selectivity of the gas products compared to the reaction using plasma only or plasma packed with γ-Al_2O_3 (Fig. 9b), but increased the total selectivity of oxygenates (Fig. 9c). For example, using Cu/γ-Al_2O_3 significantly reduced the selectivity of C_2H_6 from 17% (plasma only) to 10% but substantially enhanced the selectivity of C_2 oxygenates (9.4%). Despite relatively low changes in the CH_4 conversion among the three catalysts, the presence of these catalysts in the discharge enhanced the CH_4 conversion and energy efficiency by 70 to 85% in comparison to the plasma POM reaction without a catalyst (Fig. 9a, 9b and 9d). The enhanced performances in the plasma-catalytic POM reaction in terms of the CH_4 conversion and energy efficiency can be partly attributed to the change of the discharge characteristics induced by the catalysts (Table 2). Packing Fe/γ-Al_2O_3 into the DBD showed the highest CH_4 conversion (13%) with a maximum total liquid

selectivity of ~71%. Fe/γ-Al_2O_3 showed the highest selectivity of CH_3OH (36%) and HCHO (14.2%), followed by Cu/γ-Al_2O_3 and Ni/γ-Al_2O_3. Interestingly, compared to Cu/γ-Al_2O_3, Fe/γ-Al_2O_3 had a higher methanol selectivity but a lower selectivity towards formic acid. It is worth noting that the presence of Cu/γ-Al_2O_3 in the discharge improved the production of C_2 and C_3 long-chain oxygenates, resulting in relatively high selectivities towards CH_3COOH, C_2H_5OH and CH_3COCH_3 with a maximum CH_3COOH selectivity of ~7% (Fig. 9c). The generation of carbon-containing gaseous products (e.g., CO and C_2H_6) was closely correlated to the production of liquid products in the plasma-catalytic POM reaction. As shown in Fig. 9b, the gas selectivity for these catalysts follows the order: Fe/γ-Al_2O_3 < Cu/γ-Al_2O_3 < Ni/γ-Al_2O_3 < γ-Al_2O_3 < plasma only, in line with the opposite trend observed in the selectivity of the liquid products. Fig. S4 shows the effect of these catalysts on the yield of the gaseous and liquid products. A maximum H_2 yield of 3% was attained when using the Ni and Cu catalysts. The Fe catalyst showed the highest CH_3OH yield of ~5%, followed by Cu/γ-Al_2O_3 (3.6%), Ni/γ-Al_2O_3 (3%) and γ-Al_2O_3 (1.7%), while the highest acetic acid yield was achieved over Cu/γ-Al_2O_3. Interestingly, packing pure γ-Al_2O_3 in the DBD produced more CO_2 with the highest CO_2 yield of 0.8%.

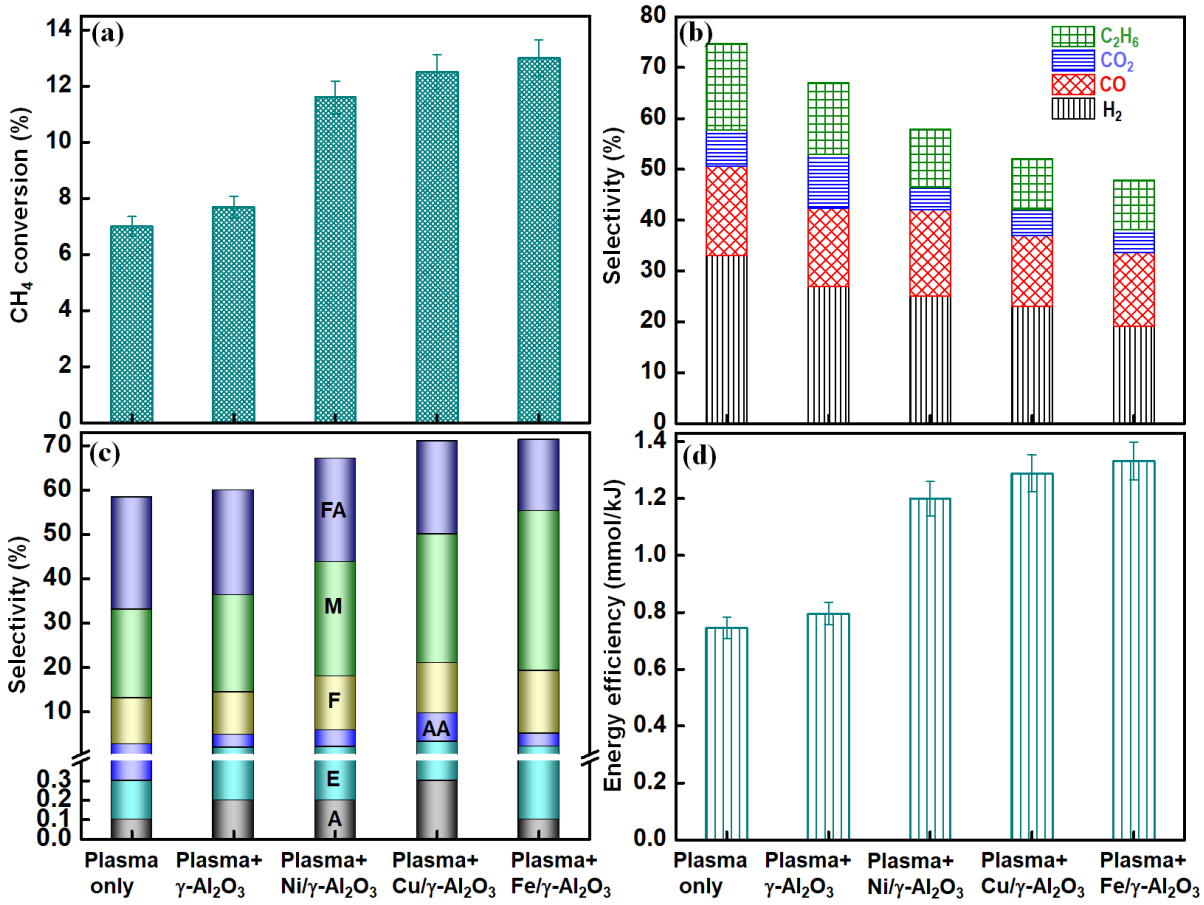

Fig. 9. Results obtained with the plasma-catalytic system compared to those with plasma only and Plasma + γ-Al_2O_3. (a) CH_4 conversion; (b) Selectivity of the gaseous products; (c) Distribution of the liquid products (FA - Formic acid (HCOOH), M - Methanol (CH_3OH), F - Formaldehyde (HCHO), E - Ethanol (C_2H_5OH), AA - Acetic acid (CH_3COOH), A - Acetone (CH_3COCH_3)); (d) Energy efficiency for CH_4 conversion (CH_4/O_2 = 5:1; Total flow rate: 30 ml min^{-1}; Power = 1.8 W; Frequency: 50 Hz).

In addition to the physical characteristics of the discharge induced by the catalyst packing, the physio-chemical properties of the catalysts also play an important role in determining the reaction performance of the plasma-catalytic POM reaction. It has been reported that transition metals (e.g. Ni, Cu, Rh) and metal complexes can strongly adsorb CH_4 and dissociate the first C-H bond with

a low energy barrier [44]. Also, it is well known that the dissociative chemisorption of CH_4 is highly dependent on the strong affinity of the metal surface to CH_4 [44]. Hence, the dissociative adsorption of CH_4 on the catalyst surface is likely to occur more easily if the metal-carbon (M-C) bond between metal oxide and CH_4 is strong [45]. The interaction between CH_4 and the catalyst surfaces was evaluated using CH_4-TPD analysis (Fig. S5). The onset desorption temperature (T_{onset}) followed the order of Fe/γ-Al_2O_3 (331 ^oC) > Cu/γ-Al_2O_3 (314 ^oC > Ni/γ-Al_2O_3 (290 ^oC) > γ-Al_2O_3 (287 ^oC). Therefore, the M-C bond strength for the catalysts (including γ-Al_2O_3 support) decreases as listed: Fe/γ-Al_2O_3 > Cu/γ-Al_2O_3 > Ni/γ-Al_2O_3 > γ-Al_2O_3. As CH_4 strongly binds to the metal oxide surface of the catalyst, its retention time in the plasma discharge zone increases, which maximize the probability for the plasma-catalytic dissociation of methane to occur. Hence, the better performance of Fe/γ-Al_2O_3 in terms of the conversion of methane and liquid selectivity can be partly contributed to the stronger M-C bond compared to that of the other catalysts. Apart from that, the selectivity of oxygenates is also affected by the acid-basic properties of the catalysts. Kalamaras et al. found that the strength and concentration of acid sites on the catalyst surfaces have a strong influence on the distribution of oxygenates in the catalytic POM reaction [33]. Han et al. reported that catalysts with more acid sites produced a higher yield of C_{2+} liquids in the POM reaction [46]. In this study, the Fe/γ-Al_2O_3 catalyst generated more methanol, but less formic acid and C_{2+} oxygenates (especially acetic acid) compared to the Cu/γ-Al_2O_3 catalyst. Higher selectivity of C_{2+} oxygenates obtained using Cu/γ-Al_2O_3 can be attributed to the presence of more acid sites on the surface of the Cu/γ-Al_2O_3 catalyst. In addition, Raham et al. highlighted that methanol could be an intermediate in the formation of formic acid in the catalytic POM to methanol [47]. Thus, over-oxidation of methanol to formic acid on the Cu catalyst surfaces could be the reason for the

decreased methanol selectivity with increased selectivity of formic acid in the plasma-catalytic POM over the Cu/γ-Al_2O_3 catalyst in comparison to Fe/γ-Al_2O_3.

3.4. Catalyst stability

To investigate the catalyst stability, the plasma-catalytic POM reaction over the Fe/γ-Al_2O_3 catalyst was carried out at room temperature and atmospheric pressure for 10 h at a constant CH_4/O_2 molar ratio of 5:1 and a fixed power of 1.8 W. Fig. 10 shows that the conversion of methane and the selectivity of gaseous products are quite stable over the 10 h reaction. However, the selectivity of CH_3COOH and HCOOH slightly increased after 6 h at the compensation of the decreased methanol selectivity, which can be attributed to the oxidation of methanol to formic and acetic acid via the intermediate acetaldehyde (CH_3CHO).

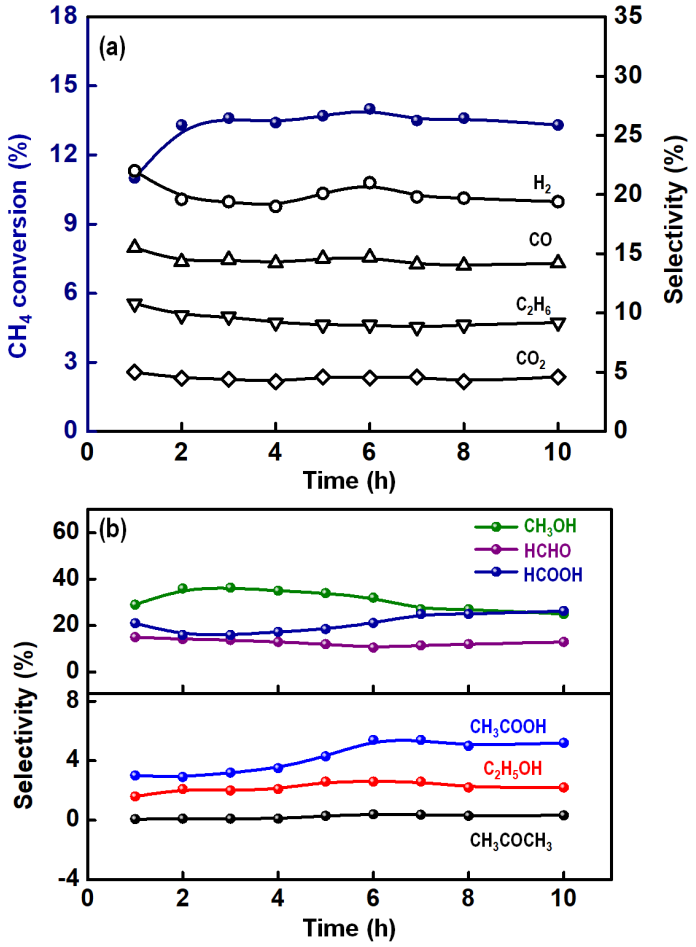

Fig. 10. Time on stream of the plasma-catalytic POM reaction over Fe/γ-Al_2O_3. (a) CH_4 conversion and selectivities of gaseous products; (b) Selectivities of liquid products.

The XRD and physisorption characterization of the spent Fe/γ-Al_2O_3 catalyst after the reaction shows that the properties of the Fe catalyst were almost unchanged before and after the reaction (Fig. 11), which further confirms the stability of the Fe catalyst during the plasma-catalytic POM reaction. Moreover, the TGA analysis of the fresh and spent catalysts (Fig. 11d) shows a weight drop at < 200 ^{o}C, which can be ascribed to the loss of moisture on the catalyst surface. There is no significant difference in the weight loss of the Fe catalyst before and after the reaction, suggesting the absence of carbon deposition on the surface of the Fe catalyst.

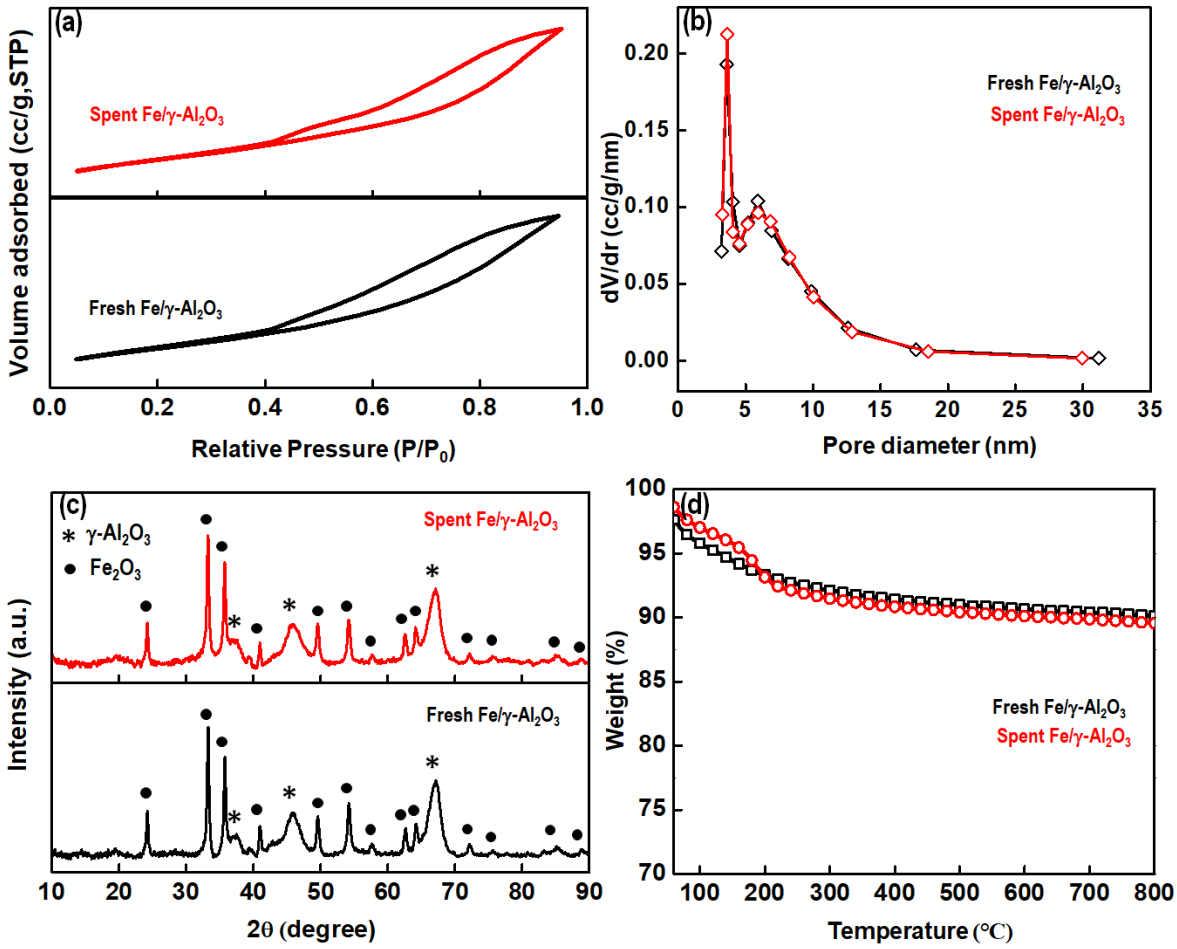

Fig. 11. Characterization of the spent Fe/γ-Al_2O_3 catalyst after running the reaction for 10 h. (a) N_2 adsorption-desorption isotherms; (b) pore size distribution; (c) XRD profiles; (d) TGA profiles.

3.4. Reaction pathways

The plasma-catalytic POM reaction involves both plasma gas-phase reactions and plasma-assisted surface reactions on the catalysts. In the plasma gas phase, the reactions are initiated through a variety of inelastic collisions between the reactants (CH_4 and O_2) and energetic electrons, generating a cascade of reactive species including radicals (e.g. CH_x and O) and excited species, which are believed to play a crucial role in the production of oxygenates. The emission

spectroscopic diagnostics (Fig. S6a) confirms the formation of a variety of reactive species in the plasma-assisted POM reaction. The emission spectrum of the CH_4+O_2 DBD shows a strong O atomic line (777.7 nm), H_α atomic line (656.6 nm) and molecular bands including CH (314 nm and 431 nm), OH (309 nm), H_2 (627-637 nm), CO (in the Angström range), CO_2 (391 nm) and C_2 (516.2 nm).

Fig. 12 illustrates the plausible reaction pathways in the plasma gas-phase reactions. The electron impact dissociation of CH_4 is considered as the major route for the initial decomposition of CH_4, resulting in the formation of CH_x (x=1, 2, 3) radicals [48]. Similarly, the electron impact dissociation of O_2 produced O atoms. Plasma chemical kinetic modeling of methane conversion showed that the R2 contributes to 79% of the total electron impact dissociation of CH_4, while R3 and R4 only account for 15% and 5%, respectively [48], which suggests that CH_3 radicals are the dominant and critical species in this reaction.

$CH_4 + e \rightarrow CH_3 + H + e$ (R2)

$CH_4 + e \rightarrow CH_2 + H_2 + e$ (R3)

$CH_4 + e \rightarrow CH + H + H_2 + e$ (R4)

The CH_4 dissociation with O atoms also contributes to the formation of CH_x species with CH_3 being the dominant radical. CH_3 radicals can recombine with themselves to form hydrocarbons (e.g., C_2H_6), or further react with energetic electrons or O radicals to produce CH_2, CH and C. The formed H atoms in the dissociation of CH_x (x=1-4) could recombine to produce H_2, one of the

main products in the gas phase. De Bie et al. reported that one of the most important routes for O_2 consumption in addition to the electron impact dissociation of O_2, is the three-body reaction of O_2 with O, H and CH_3 radicals (where the third-body can be CH_4, O_2 or H_2O). O radicals can react with CH_3 and H to form CH_3O and OH, respectively, both of which are critical intermediates in the formation of CH_3OH. Other intermediates, including CH_3O_2, CH_2O, CHO and HO_2 can also be formed [48]. The modeling results showed that the density of the radicals follows the order of CH_3O_2 > O > CH_3O > OH> CHO > CH_2OH in a 20 vol.% O_2/CH_4 DBD plasma and the formation of CH_3O_2 could be more favorable through the three-body reaction with CH_3 and O radicals [48]. In addition, Goujard et al. reported that even if the formation of gaseous products (e.g. C_{2+} hydrocarbons) via the recombination of primary radicals (e.g. CH_x, x=1-3) is fast, such reactions remain limited due to the immediate formation of oxygenated intermediates (e.g. CH_3O_2) [49]. Hence, the formation of key intermediates (e.g. CH_3O_2, CH_3O, CH_2O) is critical in the production of liquid oxygenates, such as CH_3OH and HCOOH. More C_2 oxygenates can be formed through the C-C coupling following the further reaction routes. Besides, CO and CO_2 could be produced via both oxidation of C species and de-hydrogenation of CH_xO.

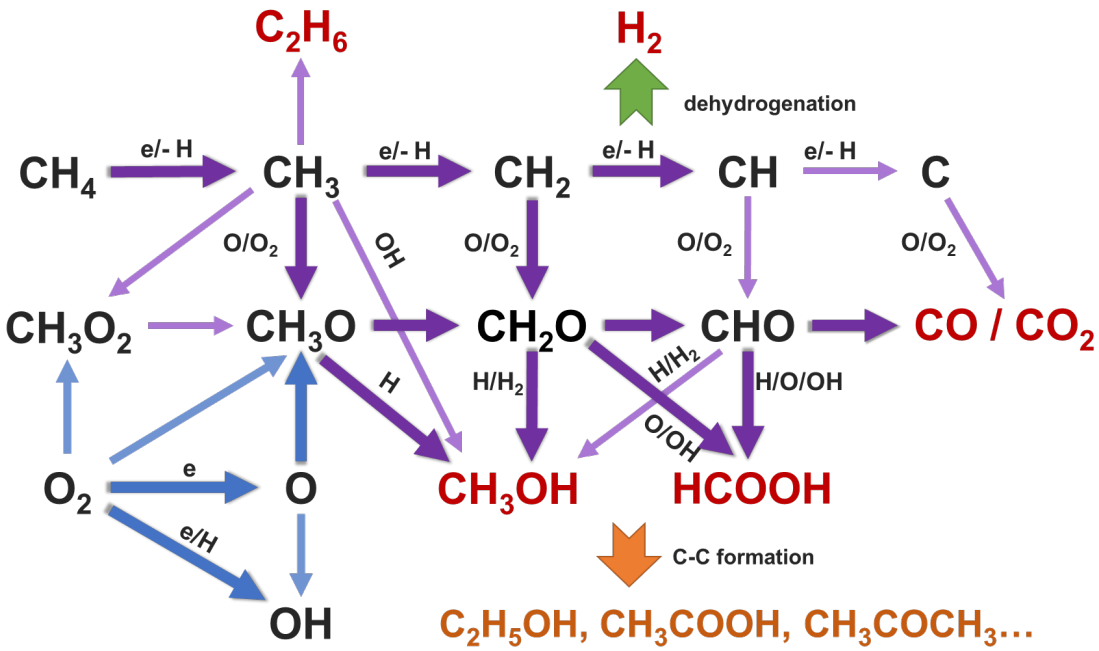

(Red: main products, Orange: C_{2+} oxygenates)

Fig. 12. Proposed reaction pathways in the plasma POM reaction without a catalyst.

Since the coupling of DBD with the catalysts significantly affects the CH_4 conversion as well as the distribution of the products (e.g., oxygenates), there must be an additional governing mechanism behind the gas-phase reactions taking place at the surface of the catalysts. Previous reports by Nozaki et al. showed that the enhanced dissociative chemisorption of vibrationally excited methane species on catalyst surfaces (Ni surface) could be the major reason behind improved methane conversion in plasma-catalytic steam reforming of methane [50]. To ascertain this, emission spectroscopic diagnostics were performed for both the plasma-only and the plasma-catalytic systems. As seen in Fig. S6b, the addition of the Fe catalyst remarkably changes the emission spectrum of the discharge. The intensity of the main characteristic peaks (CH, H, C_2, CO

and O peaks) in the spectrum of the CH_4+O_2 DBD was lower compared to that using plasma catalysis (Fe catalyst). This result can be associated with the adsorption of reactive plasma species on the catalyst surface, which has been proved to significantly reduce the intensity of the spectrum [51]. Moreover, packing the catalyst into the DBD limits the formation of filamentary microdischarges due to the reduction of the void space in the discharge gap (Fig. S7). Instead, surface discharge is dominant in the plasma-catalytic reactions, which has been well recognized in previous studies [4][52]. Moreover, the presence of a catalyst in a IPC process could change the distribution of electron energy distribution and thus produce more reactive plasma species for the reactions [53] [54].

In the plasma-catalytic surface reactions, the majority of the reactions take place via the Eley-Rideal (E-R) and Langmuir-Hinshelwood (L-H) mechanisms [19], whereas in thermal catalytic reactions, the L-H mechanism dominates. In the thermal catalytic POM reaction, CH_4 is dissociatively chemisorbed on active sites to form adsorbed CH_{4-x} species, followed by further reactions with surface adsorbed O species (generated from the adsorption and dissociation of O_2), forming syngas or methanol via carboxylate intermediate steps. However, molecular adsorption is not a spontaneous process considering the interaction potential of the molecule-catalyst system. A theoretical study by Wang et al. described radical fragments as having a much stronger interaction with metal surfaces compared to molecules, which makes radical fragments highly reactive during the chemisorption process [55].

Fig. 13 shows the possible reaction routes in the plasma-catalytic POM to the major oxygenated product (methanol) over the Fe/γ-Al_2O_3 catalyst. Surface adsorbed CH_x species are found to be crucial for methanol formation. Regarding the E-R mechanism (Fig. 13a), the key radicals, such as CH_x (x = 1, 2, 3), O and OH, formed in the gas phase, can be directly adsorbed onto the catalyst

surface. Then, the adsorbed CH_x species can be further oxidized to form CH_xO by O and OH species generated in the plasma gas-phase reactions, followed by stepwise hydrogenation on the catalyst surfaces to produce methanol. In addition, the results of CH_4-TPD analysis (Fig. S5) confirm the significance of the L-H mechanism in the plasma-catalytic POM over the Fe catalyst (Fig. 13b). The gaseous CH_4 (including its excited states) molecules could be directly adsorbed on the catalyst surface, followed by the cleavage of a C-H bond of CH_4 to form surface CH_x (x = 1, 2, 3) species. These adsorbed species can further react with other oxidative species (e.g. O and OH) present on the catalysts to form methanol directly and indirectly. It is well known that Fe-based catalysts are also effective in Fischer-Tropsch synthesis (FTS) [56]. Fe^{3+} can act as a strong adsorptive and catalytic site to activate CO molecules [57]. Therefore, the stepwise hydrogenation of CO also contributes to methanol synthesis due to the presence of syngas in the gaseous products (Fig. 9b). However, due to the relatively low concentration of CO_2 formed in this process, the contribution of CO_2 hydrogenation to methanol could be insignificant.

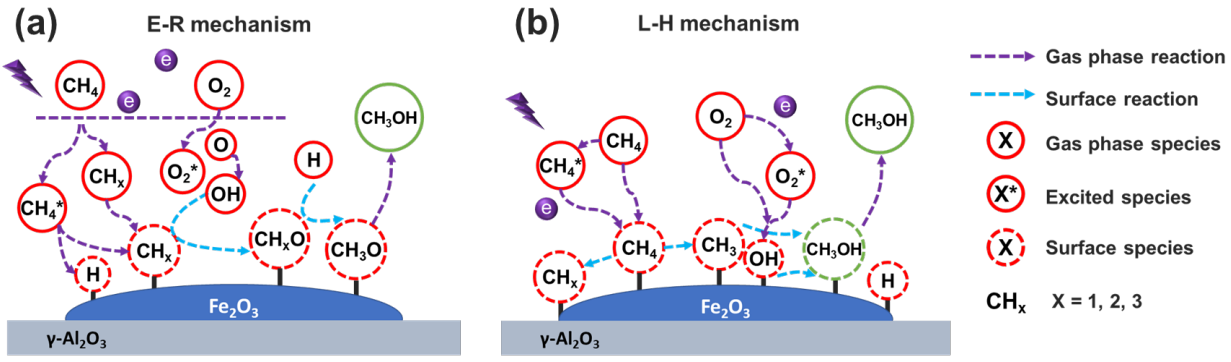

Fig.13. Proposed mechanistic routes in the plasma-catalytic synthesis of methanol on the Fe/γ-Al_2O_3 surface.

4. Conclusions

The plasma-catalytic POM for the synthesis of a range of value-added liquid fuels and chemicals has been successfully demonstrated at room temperature and atmospheric pressure. The influence of three different γ-Al_2O_3 supported transition metal oxide catalysts on the plasma-catalytic POM reaction has been investigated. Among all the catalysts, Fe/γ-Al_2O_3 catalyst was found to achieve the highest methanol selectivity of 36% followed by Cu/γ-Al_2O_3 (29%), Ni/γ-Al_2O_3 (26%) and γ-Al_2O_3 (21.8%). Compared to the plasma POM reaction without a catalyst, the combination of the plasma with the Fe/γ-Al_2O_3 catalyst almost doubled the conversion of methane with the highest methanol yield being ~5%. The presence of the Cu/γ-Al_2O_3 catalyst in the discharge considerably enhanced the selectivities of C_{2+} oxygenates including ethanol (3%) and acetic acid (6.4%), which can be attributed to the presence of more acid sites on the surface of the Cu/γ-Al_2O_3 catalyst. Both Cu/γ-Al_2O_3 and Fe/γ-Al_2O_3 catalysts were found to produce ~71% liquid fuels and chemicals. The enhanced plasma-catalytic performance for the production of oxygenates can be attributed to the plasma-enhanced surface reactions apart from the plasma gas-phase reactions, as well as the change of the discharge properties (e.g. enhanced electric field). The surface CH_x species formed through the direct adsorption from CH_x radicals in the plasma gas-phase reactions via E-R mechanism or through the dissociation of adsorbed CH_4 on the surface are found to be crucial for methanol formation.

Acknowledgements

P. Chawdhury would like to thank MHRD for supporting her fellowship. We acknowledge the European Union (EU) and Horizon 2020 funding awarded under the Marie Sklodowska-Curie Action to the EUROPAH Consortium (Grant Number 722346).

References

[1] Z. Zakaria, S.K. Kamarudin, Direct conversion technologies of methane to methanol: An overview, Renew. Sust. Energy Rev. 65 (2016) 250–261.

[2] J.H. Lunsford, Catalytic conversion of methane to more useful chemicals and fuels: A challenge for the 21st century, Catal. Today 63 (2000) 165−174.

[3] D.W. Larkin, L.L. Lobban, R.G. Mallinson, The direct partial oxidation of methane to organic oxygenates using a dielectric barrier discharge reactor as a catalytic reactor analog, Catal. Today 71 (2001) 199–210.

[4] X. Tu, J.C. Whitehead, Plasma-catalytic dry reforming of methane in an atmospheric dielectric barrier discharge: Understanding the synergistic effect at low temperature, Appl. Catal. B: Environ. 125 (2012) 439-448.

[5] C. Subrahmanyam, M. Magureanu, A. Renken, L. Kiwi-Minsker, Catalytic abatement of volatile organic compounds assisted by non-thermal plasma: Part 1. A novel dielectric barrier discharge reactor containing catalytic electrode, Appl. Catal. B: Environ. 65 (2006) 150-156.

[6] Y. Wang, Z. Liao, S. Mathieu, F. Bin, X. Tu, Prediction and evaluation of plasma arc reforming of naphthalene using a hybrid machine learning mode, J. Hazard. Mater. 404 (2021) 123965.

[7] P.M.K. Reddy, C. Subrahmanyam, Green Approach for Wastewater Treatment: Degradation and Mineralization of Aqueous Organic Pollutants by Discharge Plasma, Ind. Eng. Chem. Res. 51 (2012) 11097-11103.

[8] D. Ray, D. Nepak, S. Janampelli, P. Goshal, C. Subrahmanyam, Dry reforming of methane in DBD plasma over Ni-based catalysts: Influence of process conditions and support on performance and durability, Energy Technol. 7 (2019) 1801008.

[9] P. Chawdhury, D, Kumar, C. Subrahmanyam, NTP reactor for a single stage methane conversion to methanol: Influence of catalyst addition and effect of promoters, Chem. Eng. J. 372 (2019) 638–647.

[10] D. Mei, B. Ashford, Y. L. He, X. Tu, Plasma-catalytic reforming of biogas over supported Ni catalysts in a dielectric barrier discharge reactor: Effect of catalyst supports, Plasma Process Polymer. 14 (2017) 1600076.

[11] C. Xu, X. Tu, Plasma-assisted methane conversion in an atmospheric pressure dielectric barrier discharge reactor, J. Energy Chem. 22 (2013) 420-425.

[12] R. Vakili, R. Gholami, C.E. Stere, S. Chansai, H. Chen, S.M. Holmes, X. Fan, Plasma-assisted catalytic dry reforming of methane (DRM) over metal-organic frameworks (MOFs)-based catalysts. Appl. Catal. B: Environ. 260 (2020) 118195.

[13] L. Liu, S. Das, T. Chen, N. Dewangan, J. Ashok, S. Xi, S. Kawi, Low temperature catalytic reverse water-gas shift reaction over perovskite catalysts in DBD plasma. Appl. Catal. B: Environ. 265 (2020) 118573.

[14] L. Liu, Z. Zhang, S. Das, S. Xi, S. Kawi, $LaNiO_3$ as a precursor of Ni/La_2O_3 for reverse water-gas shift in DBD plasma: Effect of calcination temperature, Energy Convers. Manag. 206 (2020) 112475.

[15] M. Ronda-Lloret, Y. Wang, P. Oulego, G. Rothenberg, X. Tu, N. R. Shiju, CO_2 hydrogenation at atmospheric pressure and low temperature using plasma-enhanced catalysis over supported cobalt oxide catalysts, ACS Sustain. Chem. Eng. 2020, Accepted.

[16] S. Xu, S. Chansai, Y. Shao, S. Xu, Y. C. Wang, S. Haigh, Y. Mu, Y. Jiao, C. E. Stere, H. Chen, X. Fan, C. Hardacre, Mechanistic study of non-thermal plasma assisted CO2 hydrogenation over Ru supported on MgAl layered double hydroxide, Appl. Catal. B: Environ. 268 (2020) 118572.

[17] A. George, B. Shen, M. Craven, Y. Wang, D. Kang, C. Wu, X. Tu, A review of non-thermal plasma technology: a novel solution for CO_2 conversion and utilization, Renew. Sust. Energy Rev. 135 (2021) 109702.

[18] D. Mei, X. Zhu, C. Wu, B. Ashford, P.T. Williams, X. Tu, Plasma-photocatalytic conversion of CO_2 at low temperatures: Understanding the synergistic effect of plasma-catalysis. Appl. Catal. B: Environ. 182 (2016) 525-532.

[19] A. Bogaerts, X. Tu, J. C. Whitehead, G. Centi, L. Lefferts, O. Guaitella, F. Azzolina-Jury, H. H. Kim, A. B. Murphy, W. F. Schneider, T. Nozaki, J. C. Hicks, A. Rousseau, F. Thevenet, A. Khacef, M. Carreon, The 2020 plasma catalysis roadmap, J. Phys. D: Appl. Phys. 53 (2020) 443001.

[20] B. Pietruszka, K. Anklam, M. Heintze, Plasma-assisted partial oxidation of methane to synthesis gas in a dielectric barrier discharge, Appl. Catal. A: Gen. 261 (2004) 19–24.

[21] L. Song, Y. Kong, X. Li, Hydrogen production from partial oxidation of methane over dielectric barrier discharge plasma and $NiO/\gamma\text{-}Al_2O_3$ catalyst. Int. J. Hydrogen Energy 42 (2017) 19869-19876.

[22] L.M. Zhou, B. Xue, U. Kogelschatz, B. Eliasson, Partial oxidation of methane to methanol with oxygen or air in a nonequilibrium discharge plasma, Plasma Chem. Plasma Process. 18 (1998) 375–393.

[23] T. Nozaki, A. Ağıral, S. Yuzawa, J.H. Gardeniers, K. Okazaki, A single step methane conversion into synthetic fuels using microplasma reactor, Chem. Eng. J. 166 (2011) 288–293.

[24] J.J. Zou, Y.P. Zhang, C.J. Liu, Y. Li, B. Eliasson, Starch-enhanced synthesis of oxygenates from methane and carbon dioxide using dielectric-barrier discharges, Plasma Chem. Plasma Process. 23 (2003) 69-82.

[25] A. Indarto, Partial oxidation of methane to methanol with nitrogen dioxide in dielectric barrier discharge plasma: Experimental and molecular modeling, Plasma Sources Sci. Technol. 25 (2016) 025002.

[26] S. Mahammadunnisa, K, Krushnamurty, C. Subrahmanyam, Catalytic nonthermal plasma assisted co-processing of CH_4 and N_2O for methanol production, Catal. Today, 2015, 256, 102-107.

[27] L. Chen, X. Zhang, L. Huang, L. Lei, Application of in-plasma catalysis and post-plasma catalysis for methane partial oxidation to methanol over a $Fe_2O_3\text{-}CuO/\gamma\text{-}Al_2O_3$ catalyst, J. Nat. Gas Chem. 19 (2010) 628–637.

[28] A. Indarto, D.R. Yang, J. Palgunadi, J.W. Choi, H. Lee, H.K. Song, Partial oxidation of methane with Cu–Zn–Al catalyst in a dielectric barrier discharge, Chem. Eng. Process. 47 (2008) 780–786.

[29] A. Indarto, H. Lee, J.W. Choi, H.K. Song, Partial oxidation of methane with yttria-stabilized zirconia catalyst in a dielectric barrier discharge, Energy Sources. Part A 30 (2008) 1628–1636.

[30] L. Wang, Y. Yi, C. Wu, H. Guo, X. Tu, One-step reforming of CO_2 and CH_4 into high-value liquid chemicals and fuels at room temperature by plasma-driven catalysis, Angew. Chem. Int. Ed. 56 (2017) 13679–13683.

[31] D. Li, V. Rohani, F. Fabry, A.P. Ramaswamy, M. Sennour, L. Fulcheri, Direct conversion of CO_2 and CH_4 into liquid chemicals by plasma-catalysis. Appl. Catal. B: Environ. 261 (2020) 118228.

[32] S.E. Bozbag, P. Sot, M. Nachtegaal, M. Ranocchiari, J.A. van Bokhoven, C. Mesters, Direct stepwise oxidation of methane to methanol over Cu–SiO_2. ACS Catal. 8 (2018) 5721-5731.

[33] C. Kalamaras, D. Palomas, R. Bos, A. Horton, M. Crimmin, K. Hellgardt, Selective oxidation of methane to methanol over Cu- and Fe-exchanged zeolites: The effect of Si/Al molar ratio, Catal. Lett. 146 (2016) 483-492.

[34] Z. Huang, F. Cui, J. Xue, J. Zuo, J. Chen, C. Xia, Cu/SiO_2 catalysts prepared by hom- and heterogeneous deposition–precipitation methods: Texture, structure, and catalytic performance in the hydrogenolysis of glycerol to 1, 2-propanediol. Catal. Today. 183 (2012) 42-51.

[35] F.E. López-Suárez, A. Bueno-López, M.J. Illán-Gómez, Cu/Al_2O_3 catalysts for soot oxidation: Copper loading effect. Appl. Catal. B: Environ. 84 (2008), 651-658.

[36] Z. Yaakob, A. Bshish, A. Ebshish, S. Tasirin, F. Alhasan, Hydrogen production by steam reforming of ethanol over nickel catalysts supported on sol gel made alumina: Influence of calcination temperature on supports, Mater. 6 (2013) 2229–2239.

[37] S. Mosallanejad, B.Z. Dlugogorski, E.M. Kennedy, M. Stockenhuber, On the chemistry of iron oxide supported on γ-Alumina and silica catalysts, ACS Omega 3 (2018) 5362–5374.

[38] L. Pastor-Pérez, M. Shah, E. Le Saché, T.R. Reina, Improving Fe/Al_2O_3 catalysts for the reverse water-gas shift reaction: On the effect of Cs as activity/selectivity promoter, Catalysts 8 (2018) 608.

[39] I. Dahlan, N. Marsih, J. Panpranot, Gamma alumina nanotubes prepared by hydrothermal method as support of iron, cobalt, and nickel for Fischer-Tropsch catalysts, J. Chem. Mater. Res. 2 (2012) 31–38.

[40] D. Beierlein, D. Häussermann, M. Pfeifer, T. Schwarz, K. Stöwe, Y. Traa, E. Klemm, Is the CO_2 methanation on highly loaded Ni-Al_2O_3 catalysts really structure-sensitive? Appl. Catal. B: Environ. 247 (2019) 200-219.

[41] Q. Liu, X. Dong, X. Mo, W. Lin, Selective catalytic methanation of CO in hydrogen-rich gases over Ni/ZrO2 catalyst. J. Nat. Gas. Chem. 17 (2008) 268-272.

[42] R.C.R. Santos, D.M.V. Braga, A.N. Pinheiro, E.R. Leite, V.N. Freire, E. Longhinotti, A. Valentini, Role of Cu, Ni and Co metals in the acidic and redox properties of Mo catalysts supported on Al_2O_3 spheres for glycerol conversion, Catal. Sci. Technol. 6 (2016) 4986–5002.

[43] G.J.M. Hagelaar, L.C. Pitchford, Solving the Boltzmann equation to obtain electron transport coefficients and rate coefficients for fluid models, Plasma Sources Sci. Technol. 14 (2005) 722.

[44] Y.Q. Su, J.X. Liu, I.A. Filot, L. Zhang, E.J. Hensen, Highly active and stable CH_4 oxidation by substitution of Ce^{4+} by two Pd^{2+} ions in CeO_2 (111), ACS Catal. 8 (2018) 6552–6559.

[45] Y. Tsuji, K. Yoshizawa, Adsorption and activation of methane on the (110) surface of rutile-type metal dioxides, J. Phys. Chem. C. 122 (2018) 15359-15381.

[46] S. Han, D.J. Martenak, R.E. Palermo, J.A. Pearson, D.E. Walsh, The direct partial oxidation of methane to liquid hydrocarbons over HZSM-5 zeolite catalyst, J. Catal. 136 (1992) 578–583.

[47] A.K.M. Lutfor Rahman, M. Kumashiro, T. Ishihara, Direct synthesis of formic acid by partial oxidation of methane on H-ZSM-5 solid acid catalyst, Catal. Comm. 12 (2011) 1198-1200.

[48] C. De Bie, J. van Dijk, A. Bogaerts, The dominant pathways for the conversion of methane into oxygenates and syngas in an atmospheric pressure dielectric barrier discharge. J. Phys. Chem. C. 119 (2015) 22331-22350.

[49] V. Goujard, T. Nozaki, S. Yuzawa, A. Ağiral, K. Okazaki, Plasma-assisted partial oxidation of methane at low temperatures: numerical analysis of gas-phase chemical mechanism, J. Phys. D: Appl. Phys. 44 (2011) 274011.

[50] T. Nozaki, N. Muto, S. Kado, K. Okazaki, Dissociation of vibrationally excited methane on Ni catalyst: Part 1. Application to methane steam reforming. Catal. Today, 89 (2004) 57-65.

[51] L. Wang, Y. Yi, H. Guo, X. Tu, Atmospheric pressure and room temperature synthesis of methanol through plasma-catalytic hydrogenation of CO_2, ACS Catal. 8 (2017) 90–100.

[52] Y. Wang, M. Craven, X. Yu, J. Ding, P. Bryant, J. Huang, X. Tu, Plasma-enhanced catalytic synthesis of ammonia over a Ni/Al_2O_3 catalyst at near-room temperature: Insights into the importance of the catalyst surface on the reaction mechanism. ACS Catal. 9 (2019) 10780-10793.

[53] X. Tu, H. J. Gallon, J. C. Whitehead, Electrical and spectroscopic diagnostics of a single-stage plasma catalysis system: Effect of packing photocatalyst TiO_2, J. Phys. D: Appl. Phys., 44 (2011) 482003.

[54] L. Liu, Z. Zhang, S. Das, S. Kawi, Reforming of tar from biomass gasification in a hybrid catalysis-plasma system: A review, Appl. Catal B: Environ. 250 (2019) 250-272.

[55] G.C. Wang, Y.H. Zhou, Y. Morikawa, J. Nakamura, Z.S. Cai, X.Z. Zhao, Kinetic mechanism of methanol decomposition on Ni (111) surface: a theoretical study, J. Phys. Chem. B, 109 (2005) 12431-12442.

[56] D.B. Bukur, X. Lang, Highly active and stable iron Fischer-Tropsch catalyst for synthesis gas conversion to liquid fuels, Ind. Eng. Chem. Res. 38 (9) (1999) 3270–3275.

[57] C. Pirola, C.L. Bianchi, A. Di Michele, S. Vitali, V. Ragaini, Fischer-Tropsch and water gas shift chemical regimes on supported iron-based catalysts at high metal loading, Catal. Comm. 10 (2009) 823–827.

Graphical Abstract